Earth Syst. Dynam. Discuss., doi:10.5194/esd-2016-37, 2016
Manuscript under review for journal Earth Syst. Dynam.
Published: 29 August 2016

Earth System Dynamics Discussions
Open Access
EGU

A network-based detection scheme of the jet stream core

Sonja Molnos[1,2], Tarek Mamdouh[3], Stefan Petri[1], Thomas Nocke[1], Tino Weinkauf[4], Dim Coumou[1]
[1] Potsdam Institute for Climate Impact Research, Potsdam, Germany
[2] Department of Physics, University of Potsdam, Germany
[3] Ain Shams University, Egypt
[4] KTH Royal Institute of Technology, Sweden

Correspondence to: S. Molnos(molnos@pik-potsdam.de)

Abstract. The polar and subtropical jet streams are strong upper-level winds with a crucial influence on weather throughout the Northern Hemisphere mid-latitudes. In particular, the polar jet is located between cold Arctic air to the North and warmer sub-tropical air to the South. Strongly meandering states therefore often lead to extreme surface weather. So far algorithms to detect jets' core around the hemisphere, including strong North-South undulations, are lacking. We develop a network-based scheme using Dijkstra's shortest path algorithm to detect the polar and subtropical jet stream core. This algorithm considers not only the commonly used wind strength for core detection but also takes wind direction and climatological latitudinal position into account. Furthermore, it distinguishes between polar and subtropical jet, and between separate and merged jet states.

The detection scheme is optimized using simulated annealing and compared against an algorithm developed by Rikus (Rikus, 2015). After the successful optimization process we apply our scheme to climatology data and analyse seasonal data sets.

We present probabilistic, regionally distinct positions for both jets for all seasons. This shows that winter is characterized by two well separated jets at mean longitudes of 20°S and 140°N. In contrast, summer normally has a single merged jet over the western Hemisphere and both merged and separated jet states possible in the eastern Hemisphere.

With this algorithm it is possible to investigate the position of the jets' cores around the hemisphere and is therefore well suitable for analyses of jet stream patterns in observations or models.

Keywords:

Upper tropospheric jets, detection scheme, probability analysis of the jet stream cores

1 Introduction

Jet streams are upper-level fast currents of air that circulate and meander around the hemisphere and play a kay role in the general circulation of the atmosphere as well as in generating weather conditions throughout the Northern Hemisphere mid-

Earth Syst. Dynam. Discuss., doi:10.5194/esd-2016-37, 2016
Manuscript under review for journal Earth Syst. Dynam.
Published: 29 August 2016

latitudes. In general, we distinguish between two jet stream types in the troposphere: the subtropical jet stream (STJ) and the polar front jet stream or, simply, the polar jet stream (PFJ).

The STJ is located at the upper branch of the Hadley circulation and forms due to momentum conservation, when air moves poleward, and meridional contrasts in solar heating (Woollings et al., 2010). The PFJ is situated along the polar front and is driven by baroclinic eddies that evolve due to temperature gradients along the region of the polar front (Pena-Ortiz et al., 2013) and is therefore often referred to as eddy-driven jet. Those transient eddies transport heat and vorticity and thereby accelerate the westerly winds (Woollings, 2010). The hemispheric north-south temperature gradient is strongest in winter and weakest in summer and this can explain variations in the jet stream strength and position between seasons. In summer, the winds are weaker and the jets move farther polewards, whereas in winter the winds are stronger and the jets move farther equatorwards as the cold front extends into subtropical regions (Ahrens, 2012).

Jet streams are thus sensible to changes in temperature gradient and variability and hence also to climate change (Barnes and Polvani, 2013; Grise and Polvani, 2014; Solomon and Polvani, 2016). Large-scale undulations in the jets (Rossby waves) could sometimes become quasi-stationary (i.e. stagnant) which can lead to persistent weather conditions at the surface. Persistent weather can favour some type of extreme weather events (Coumou et al., 2014; Stadtherr et al., 2016). Petoukhov et al. (2013) proposed a mechanism that could provoke such weather extremes in the Northern Hemisphere mid-latitudes. Quasi-stationary Rossby waves in summer linked to persistent heat waves and severe floods (Petoukhov et al., 2013, 2016). Likewise in winter, strongly meandering jets, driven either by anomalous tropical (Palmer, 2014; Trenberth et al., 2014) or extratropical (Peings and Magnusdottir, 2014) sea-surface temperatures or stratospheric variability (Cohen et al., 2014; Kretschmer et al., 2016), can lead to mid-latitude cold spells.

Hence, jet streams play a key role in the general circulation and for generating our weather conditions.

Several schemes have been proposed to extract the jet stream from wind data, each with advantages, but also limitations.

For example, Rikus developed a detection-method to analyse zonal mean positions of the jet streams (Rikus, 2015). It uses the zonally averaged wind in latitude – height space to identify with the help of a closed contour object identification scheme the cores of the jet streams. This method thus cannot analyse the development of the jet stream in longitudinal East-West direction.

Gallego at al. developed a more advanced scheme using a geostrophic streamline of maximum daily averaged velocity at 200 hPa to define the jet stream in the Southern Hemisphere (Gallego et al., n.d.). The algorithm defines jet streams as strong winds with wind velocities higher than 30 $m\,s^{-1}$ and distinguishes between the subtropical and polar jet stream, when the average latitudinal difference is less than 15°. This threshold was set by manual optimization. However, since the strength of the jet stream can change rapidly on weekly timescales, the jet stream core should be independent of an absolute wind velocity threshold.

The first 3D method (i.e. longitude, latitude and height) was developed by Limbach at al. (2012). They implemented a method to detect and track specific properties of atmospheric features as merging and splitting jet streams (via clustering of data points), but it cannot distinguish between subtropical and polar jet stream and used also a wind velocity threshold .

Earth Syst. Dynam. Discuss., doi:10.5194/esd-2016-37, 2016
Manuscript under review for journal Earth Syst. Dynam.
Published: 29 August 2016

A different 3D detection scheme was developed by Pena-Ortiz et al. (2013) which identifies local wind maxima in the zonally wind field at each grid point and each day by using a specified wind speed threshold. The algorithm distinguishes between the subtropical and polar jet stream via a specified threshold in latitude. A limitation of such approach is that the value of these thresholds (in wind speed and latitudinal separation) is not well defined. In particular the polar jet, which is our prime interest, can meander over large latitudinal ranges and experience strong variability in its strength.

To overcome these issues, we propose a new method which is based upon Dijkstra's Shortest Path algorithm to find the shortest path in an edge cost function, which can be defined freely by any combination of relevant variables. We develop a 2D detection scheme for both the PFJ and STJ core, and define our edge cost function using wind speed, wind direction, and a latitudinal guidance parameter (which is not thresholded). This way, we are able to accurately differentiate between subtropical and polar jet.

In section 2 we describe the data used in this algorithm. In section 3 we explain the mechanism of our detection scheme and in section 4 explain the optimization process and its results. Afterwards (section 5), we analyse jet stream positions since 1979 and calculate their probability density functions for all different seasons. We conclude with a summary and a discussion in section 6.

2 Data

In this study, we used ERA-Interim data (Dee et al., 2011) from the European Centre for Medium-Range Weather Forecasts (ECMWF). The ECMWF provides meridional and zonal wind velocity components with a 0.75 latitude-longitude grid resolution. We chose 11 vertical layers of the upper troposphere stretching from 500 mb to 150 mb and for 4 time snap shots per day (0:00h, 6:00h, 12:00h, 18:00h) for the years 1979–2014. From this data, we calculate 15 - day running mean and vertically averaged (mass-weighted) wind velocity, which is used for all analysis in this paper.

In the following text, a "time step" denotes a 15 - day average centred on a given day.

3 Methods

Our jet stream core detection scheme is based on Dijkstra's shortest path algorithm, which is a widely used method for finding the shortest path from a source to a destination within an edge-weighted graph (Dijkstra, 1959). We assume that the jet stream core is a closed path along the hemisphere, source (most westerly point) and destination (most easterly point) are at the same location.

We use wind data on a 2-dimensional grid of the northern hemisphere. Each grid point is taken as a node in a network graph. Only geographically adjacent grid points respectively nodes are connected via edges and thus no teleconnections are considered. The nodes within the most westerly column are copied after the end of the most easterly column to ensure that

Earth Syst. Dynam. Discuss., doi:10.5194/esd-2016-37, 2016
Manuscript under review for journal Earth Syst. Dynam.
Published: 29 August 2016

that the path found with Dijkstra's algorithm starts and ends at the same location. The path itself is not restricted to a forward direction such that the path could pass multiple times same longitudinal coordinates.

To avoid noise and reduce computational costs, only those grid points are connected, where the wind velocity is greater than 10% of the maximum wind velocity for the considered time step.

In order to reduce computational costs, the spatial domain is reduced to the main region of interest 30°N–90°N for the polar jet stream, and 0°–75°N for the subtropical jet stream on the northern hemisphere (something which does not affect the results).

We define an edge cost function C_j based upon wind speed, wind direction and a latitudinal guidance-function using the climatological mean latitudinal position of each jet:

$$C_j = w_1 X_j + w_2 Y_j + w_3 Z_j, \qquad w_1 + w_2 + w_3 = 1 \tag{1}$$

The variables X_j, Y_j and Z_j, each normalized to the interval [0,1], are the three terms for computation of the cost at edge e_j and w_1, w_2 and w_3 are the weights that control the contributions of the three cost terms. These weights sum up to one as well, i.e. w_1, w_2 and w_3 are non-negative and their sum is less than or equal to one.

The three terms and their respective factors are illustrated in Fig. 1(a-b). Figure 1(a) shows all nodes and edges as well as the wind velocities of the considered node (blue arrows) in the grid. For each edge e_j, its cost is computed depending on the wind velocities (term X_j, length of blue arrows) and wind directions (term Y_j, angle between blue arrow and black edge) at its two nodes A and B and from its latitude (term Z_j, shown in Fig. 1(b)).

The first term X_j captures the magnitude of the wind field at the nodes A and B. Jet streams are strong upper-level winds and hence the jet stream core should be there, where the wind strength is maximal:

$$X_j = 1 - \frac{\sqrt{{u_A}^2 + {v_A}^2} + \sqrt{{u_B}^2 + {v_B}^2}}{2 \max_{k=1}^{n}(\sqrt{{u_k}^2 + {v_k}^2})}, \tag{2}$$

whereby u_A, u_B, v_A and v_A are the zonal and meridional wind speeds at nodes A and B connected by edge j and $\max_{k=1}^{n}(\sqrt{{u_k}^2 + {v_k}^2})$ is the maximum wind speed found at the considered time step for any node k (see also Fig. 1(a)). The second term in Eq.(2) is thus always smaller than or equal to 1. We subtract this value from 1, and thus low values of X_j refer to high wind speeds, because Dijkstra's algorithm will minimize the edge cost of the path (i.e. find the shortest path).

The second term Y_j weights each edge $\boldsymbol{e}_j$ according to the angle between the normal vector of the edge and the wind

Earth Syst. Dynam. Discuss., doi:10.5194/esd-2016-37, 2016
Manuscript under review for journal Earth Syst. Dynam.
Published: 29 August 2016

Earth System Dynamics Discussions Open Access EGU

direction:

$$Y_j = \frac{1 - |\boldsymbol{V}_A| \cdot |\boldsymbol{e}_j|}{2} \quad (3)$$

Here $|V_A|$ is the normalized vector of the wind direction in node *A* and $|\boldsymbol{e}_j|$ is the normalized vector of the edge direction (see also Fig. 1(a)).

The third term Z_j is used to differentiate between Polar and Subtropical jet streams. Basically, it favours pathways that are close to the climatological mean latitude of polar and subtropical jet but still allows free movement within a latitudinal belt of roughly $\pm 20\%$ of the climatological mean. Outside this latitudinal belt, Z rapidly grows according to

$$Z_j = \frac{(\phi_j - \phi_{\text{clim}})^4}{\max(\phi_{\text{clim}}, 90 - \phi_{\text{clim}})^4} \quad (4)$$

Hereby, ϕ_j and ϕ_{clim} are the latitude of the edge and of the climatological mean latitude, respectively.

The reason for taking the difference between the latitudes raised to the power 4 is to give flexibility to the detected path to move almost freely in the vicinity of the desired latitude, but a strongly increasing weight farther away. This is also illustrated in Fig. 1(b), where the condition Z_j for the STJ and PFJ is shown.

After calculating the edge cost for each edge according to Eq.(1), our algorithm returns from the set of all possible paths P_i with total edge costs of the path TC_i the path P_{min} with minimal total edge cost TC_{min}:

$$TC_{\text{Min}} = \text{Min}(TC_i) = \text{Min}\left(\sum_{j=0}^{n} \text{C}_\text{j},\right) \quad (5)$$

where *n* is the number of edges in the path P_i.

4 Calibration and testing

The results found with our algorithm, and therefore the paths of the jet stream are sensitive, to the chosen weights w_1, w_2 and w_3 and the climatological latitude ϕ_{clim} as for example shown in Fig. 2.

The detected PFJ path is very similar to the STJ path, which is explained by strong subtropical wind speeds. As clearly seen in the right panel of Fig. 2, the PFJ core is actually located near of 65°N.

Clearly a parameter-optimization is needed to avoid such unrealistic results.

Earth Syst. Dynam. Discuss., doi:10.5194/esd-2016-37, 2016
Manuscript under review for journal Earth Syst. Dynam.
Published: 29 August 2016

The outlines of this calibration scheme are shown in Fig. 3 : Dijkstra's algorithm finds the shortest path of the jet stream in a network graph. For defining the edge cost for each edge in the graph, we have 3 terms, which were explained in detail before. However, we have to find optimal values for weights w_1, w_3 and for ϕ_{clim}.

To solve this problem, we use Simulated Annealing to optimize the parameters w_1, w_3 and ϕ_{clim} and define a zonal mean skill function calibrating against Rikus' algorithm (explained in the next section).

With Dijkstra's algorithm we resolve jet stream positions in a graph that is constructed from a 2D grid (longitude *and* latitude) and thus provides a range of latitudinal positions. We expect the mean of all latitudinal positions to be close to the zonal mean jet position found by Rikus' algorithm and thus define our skill function accordingly (Eq. (6)).

We determined the wind direction weight w_2 manually, since it only smooths the curve locally and therefore does not affect the zonal mean position used for tuning.

4.1 Rikus' algorithm

Rikus' algorithm is a closed contour object identification scheme (Rikus, 2015). It operates on a zonal mean zonal wind and treats the two dimensional (pressure height and latitude) zonal mean U field for every time step as a single isolated image using image coordinates defined by *x*- and *y*-position.

Figure 4 shows the scheme of Rikus' algorithm. First a maximum (minimum) filter is applied to the original zonal mean U field, which calculates the 25 point maximum stencil (25 point minimum stencil) of the field. Therefore, the algorithm replaces the maximum (minimum) value within a box of 5 points in *x*- and *y*- direction (resulting in a total 25 grid points) to the central grid point of that box. This way the fields U_{Min} and U_{Max} are determined (Fig. 4 b, c).

In a second step Rikus' algorithm examines for each point whether $U_{\text{Max}}(x,y) - U_{\text{Min}}(x,y) > 0.4$ and whether $U_{\text{Max}}(x,y) = U(x,y)$ (Fig. 4 d, e). Only points where both conditions are fulfilled are zonal mean jet stream cores (Fig. 3f, blue points).

We applied Rikus' algorithm to the zonal mean zonal wind field of each time step (i.e. 15 - days running mean ERA-Interim data (Dee et al., 2011)) to identify the zonal mean jet stream latitude for all levels and latitudes in the domain 150mb–430mb and 50°N–70°N (15°N–50°N) for the years 1979–2014. We selected those days, where one polar and/or one jet stream within the above mentioned region were found. We used this Rikus' algorithm in a skill function to be minimized with simulated annealing (explained in the next section) to calibrate the weights of Eq. (1).

4.2 Simulated Annealing

We calibrated the detection of the polar jet stream with the optimization algorithm "Simulated Annealing" (Kirkpatrick, 1984), implemented in the multi-run simulation environment SimEnv. (Flechsig et al., 2013).

This approximates the global minimum of a high-dimensional skill score function.

Our goal is to minimize the mean square error function between the mean latitude of the jet stream calculated with Dijkstra's

Earth Syst. Dynam. Discuss., doi:10.5194/esd-2016-37, 2016
Manuscript under review for journal Earth Syst. Dynam.
Published: 29 August 2016

Earth System Dynamics Discussions

algorithm and the zonal-mean latitude computed with Rikus' algorithm (Rikus, 2015):

$$S = \sqrt{(\phi_{\text{Rikus}} - \phi_{\text{mean}})^2} \quad (6)$$

The reason for tuning our spatially resolved tool to a zonal mean approach is that the characteristics of the jet stream like the zonal mean latitude position should be ultimately the same. The mean latitude detected by our algorithm should be very close to the maxima in zonal mean zonal wind.

With the found zonal mean subtropical and polar jet stream latitudes by Rikus we optimized the parameters w_1, w_3 and ϕ_{clim} for cold (November, December, January, February, March, April) and warm months (May, June, July, August, September, October). Rikus' algorithm finds a subtropical jet for almost all time steps, we used at first every 14$^{\text{th}}$ time step found subtropical jet stream core for optimization. In the second step we used every found point and used as start point the optimized parameters found by the first step. Otherwise the optimization process would take a long time. For the polar jet stream, we used all jet stream cores found by Rikus' algorithm.

As starting point for our automatic optimization scheme the parameters (w_1, w_3 and ϕ_{clim}) of the graph for Dijkstra's algorithm were set to manually selected values as listed in Table 1.

4.3 Results of the optimization process

The results of our automatic optimization scheme are listed in Table 1. The jet stream guidance parameter w_3 needs to have a strong weight in order to separate the STJ and the PFJ. For the detection of individual jet streams a large value of w_3 is admissible, because the quantity Z_j is a quartic function, which is very small in the vicinity $(\pm 20\%)$ of ϕ_{clim} (see Fig. 1(b)).

The climatological mean latitude ϕ_{clim} shifts poleward in the warm season for both subtropical and polar jet, reflecting the seasonal cycle.

The zonal-mean latitudinal difference between Dijkstra (a longitudinal resolved latitude) and Rikus (a zonal mean latitude) for the subtropical jet stream (<2°) is always smaller than the difference for the polar jet stream (<5°). This difference is expected to be larger for the PFJ, because it is more undulated, whereas the STJ is strongly zonally oriented.

Improvements of the jet stream cores due to the optimization process relative to jet stream cores found by the untuned algorithm (Fig. 2) are illustrated in Fig. 5. Here, the left panels show the zonal mean latitude of the jet stream core calculated with Dijkstra's algorithm (light blue lines) and that computed by Rikus' algorithm (blue circles). The black solid (dashed) lines are the borders of the PFJ (STJ) core latitudinal positions as detected with Dijkstra's algorithm around the hemisphere.

After tuning, the zonal mean latitude of the polar jet stream core detected with Dijkstra's algorithm is close to the latitude computed by Rikus' algorithm (compare Fig. 5 with Fig. 2). Moreover, visual inspection of the right panel of Fig. 5 illustrates that our algorithm now correctly finds the polar jet around the hemisphere.

Earth Syst. Dynam. Discuss., doi:10.5194/esd-2016-37, 2016
Manuscript under review for journal Earth Syst. Dynam.
Published: 29 August 2016

The mean latitude calculated with Dijkstra's algorithm does not always match perfectly with the mean latitude computed by Rikus' algorithm, because the first is a 2D–algorithm in longitude and latitude and the latter is a 2D–algorithm in latitude and height. Rikus' algorithm therefore does not capture the undulations of the jet stream.

Often any such differences are related to the existence of not one but two zonal-mean PFJ maxima. For example in Fig. 6 there exists a zonal mean maximum at latitude ~55°N and another maximum at ~73°N (left panel) but this is due to the undulation features of the jet stream pattern (right panel). Our algorithm accurately resolves that undulation pattern, whereas Rikus' only detects the stronger southerly maxima, since it searches in the ranges between 50°N and 70°N for the polar Jet stream. For that reason its mean latitude is in between the two maxima.

In other cases a zonal-mean maximum found by Rikus' algorithm exists only in one longitudinal range. For example, in Fig. 7 the maximum of the pressure-height- latitude plot exists mainly because of the region between $0°E - 100°E$ and around $70°N$ latitude. Since in other parts a different path represents the polar jet stream, the mean jet stream cores are not the same.

An example, in which the PFJ core shows a high-over-low-blocking situation, is shown in Fig. S1 (supplementary materials).

In Fig. 8 the differences between the zonal mean polar jet stream cores calculated by Rikus' algorithm and with Dijkstra's algorithm are shown in two different subplots. Panel (a) shows a day-year plot depicting in blue days for which Rikus' algorithm finds a polar jet stream in agreement with the range of jet stream core latitudes detected with Dijkstra's algorithm. In yellow are those days, where Rikus' polar jet stream core position is not between minimum and maximum latitude of the polar jet stream path detected with Dijkstra's algorithm. These are 199 of 3122 data points which is equivalent of 6.4%. Figure 8 (b) shows the difference between the mean latitude calculated by Rikus' and the mean latitude calculated with Dijkstra's algorithm. The mean of the difference is 5°, but there are also some cases, where the difference is much higher, up to 20°. These differences are due to the undulations as we explained in the other plots.

The day–year plot of the subtropical jet stream in Fig. 9 shows that every single time step Rikus' latitude position is within the range of latitudes found with Dijkstra's algorithm. Figure 9(b) indicates the difference between the mean latitude calculated by Rikus' and the mean latitude calculated with Dijkstra's algorithm, which is very small. The mean is 2° and the highest values are 6°.

5 Jet stream probability analysis

In this section we present some results of the analysis of the jet stream paths that were detected by our algorithm.
Figures 10, 11, 12, 13 and 14 show probabilistic jet stream positions for the annual mean and for different seasons with brown dashed contour lines representing the subtropical jet and black solid contour lines representing the polar jet.

Earth Syst. Dynam. Discuss., doi:10.5194/esd-2016-37, 2016
Manuscript under review for journal Earth Syst. Dynam.
Published: 29 August 2016

The seasonal cycle of the STJ is clearly seen with winter latitudes between 20° and 40° latitudes and summer latitudes further north. Moreover, in summer the jets merge in the western hemisphere, whereas in winter they are clearly separated over almost all longitudes.

The probability frequency of the PFJ is much broader than the probability of the STJ and no clear latitudinal shift between seasons is observed. In particular in summer the PFJ distribution is smeared out (indicating large fluctuations in its position) whereas in winter it is more confined.

This strong meandering of the eddy-driven PFJ is explainable due to the nature of wave-mean flow-feedbacks (Harnik et al., 2014). The PFJ cores lie always between 40°N-80°N, only in longitudinal direction there is a seasonal dependence. Over Asia the probability of a high-latitude PFJ is larger in summer than in winter. Over Europe the probability of a low latitude PFJ is higher in summer. This is also observable for East Pacific and America, but less pronounced, instead there seem to be in spring and summer two preferable states: merged jet state with a jet at ca. 50°N and a second state with two jets at respectively ca. 50°N and ca 70°N.

In general the probability of PFJ at low latitude is small over the European sector compared to other regions and therefore double jet states occur in every season here. In North America such a clearly separated STJ and PFJ is only observed in winter.

The annual plot shows again that clearly separated jet states are more frequently detected over Europe.

This coexistence of STJ and PFJ in the eastern hemisphere compared to more frequent merged jet states in the western hemisphere, is well documented in the literature, but was never shown in probabilistic plots as presented here (Eichelberger and Hartmann, 2007; Li and Wettstein, 2012; Son and Lee, 2005; Woollings, 2010). Those different jet stream states occur, since the processes which lead to the existence of STJ and PFJ, operate and interact continuously (Harnik et al., 2016; Lee and Kim, 2003). In the North Atlantic STJ and PFJ are separated, because the region of strongest baroclinicity is located relatively far poleward. In contrast, the region of strongest baroclinicity in the North Pacific is located near the latitude of maximum zonal wind favouring a merged jet (Lee and Kim, 2003; Li and Wettstein, 2012). Such a merged jet stream is also called eddy-thermally driven jet because of the two different genesis mechanisms. In special cases there is the possibility that this eddy-thermally driven jet stream also appears over the North Atlantic (Harnik et al., 2014). This happens, if the tropical forcing strengthens or the mid-latitude baroclinicity is weakening.

In addition, the panels (b) give probabilities of the zonal-mean latitude of both jets showing enhanced variability of the PFJ compared to the STJ. The range of overlapping latitudes between STJ and PFJ is larger in summer than in winter, because of the poleward shift of the STJ. The variability in STJ is lower in summer and in winter than for spring and autumn, whereas the probability distribution of the PFJ is similar between seasons. However, the location of the maximum in the PFJ histogram changes per season: In winter the maximum is at ca 55°N, whereas in summer there are two maxima at 50°N and at 70°N. These two maxima probably reflect the different behaviour in western and eastern hemisphere in the PFJ. In spring there is no clear maximum visible (between 40°N-60°N) and in autumn it is again close to 55°N.

In the annual plot more homogenous distributions of the STJ and PFJ is seen. This is expected due to the seasonal cycle.

Earth Syst. Dynam. Discuss., doi:10.5194/esd-2016-37, 2016
Manuscript under review for journal Earth Syst. Dynam.
Published: 29 August 2016

For verification, we compare the probabilistic jet fields with seasonal climatological wind fields (Panels (c)). In general, all probability density functions (PDFs) of the jet stream cores in their respective seasons coincide well with the wind fields. In summer the wind field magnitude is very low and more homogeneously spread other the hemisphere. In summer the jet stream cores are farther North than in winter due to the weaker temperature gradient in summer. In general the gradient of the wind velocities as well as the strength of the velocities in summer are weaker than in winter.

6 Summary and Discussion

We have proposed a novel and objective method to detect the subtropical and polar jet stream cores. Our method uses a graph approach employing Dijkstra's shortest path algorithm. With this method we are able to describe both spatially separated as well as merged jet stream cores. If the subtropical and polar jets merge, the two detected jet stream cores become very close to each other.

We used three terms to define the edge costs: wind magnitude, wind direction and a jet stream latitudinal guidance term. Based on that, the algorithm finds jet stream core as a closed path. Parameters entering this detection scheme were optimized using simulated annealing and comparing our spatially resolved scheme with a zonal-mean detection scheme to avoid unrealistic results. We show that the zonal-mean jet stream properties are in good agreement.

In addition, we calculate the probabilities of the northern STJ and PFJ core and show that the probability of two clearly separated jet streams is very high over East Atlantic and Eurasia and very low over the Pacific and America. This is consistent with previous studies (Li and Wettstein, 2012; Son and Lee, 2005). The underlying reason is the different location of strongest baroclinicity between the North Pacific and the North Atlantic. In the former, the strongest baroclinicity is located near the latitude of the maximum zonal wind and in the latter the it is located relatively far poleward. The histograms of STJ and PFJ density for different seasons and for the annual mean show that the latitudinal variability of the PFJ is much larger than the variability of the STJ. This much larger variability is due to the nature of wave-mean flow-feedbacks (Harnik et al., 2014).

For future work we plan to extend the algorithm in three-dimension and apply it to the Southern hemisphere in order to compare the results.

Furthermore, we intend to analyze the influence and impacts of the jet stream to extreme events using cluster analysis. This way, we can examine the link of particular cluster patterns to extreme weather events and determine which jet stream patterns has a higher probability for extremes. In addition we plan to find possible drivers, which lead to those jet stream patterns using causal effect networks (Kretschmer et al., 2016).

Another possibility is to apply our method to model data such as CMIP5 in order to analyze, whether models can reproduce the jet accurately.

Code and data availability

Code and data are stored in PIK's long term archive, and are made available to interested parties on request.

Team list

S. Molnos, T. Mamdouh, S. Petri, T. Nocke, T. Weinkauf, D. Coumou

Author contribution

S. Molnos, T. Mamdouh, T. Weinkauf and D. Coumou developed the study Conception. T.Weinkauf, T. Mamdouh and T.Nocke developed the analysis method. S.Molnos, S. Petri and T. Mamdouh developed the model code and performed the simulations. S. Molnos and D. Coumou analysed and interpreted the data. S. Molnos prepared the manuscript with contributions from all co-authors.

Competing interests

The authors declare that they have no conflict of interest.

Acknowledgements

We thank ECMWF for making the ERA-Interim available. The work was supported by the German Federal Ministry of Education and Research, grant no. 01LN1304A, (S.M., D.C.). The authors gratefully acknowledge the European Regional Development Fund (ERDF), the German Federal Ministry of Education and Research and the Land Brandenburg for supporting this project by providing resources on the high performance computer system at the Potsdam Institute for Climate Impact Research.

References

Ahrens, C. D.: Meteorology Today: An introduction to weather, climate, and the environment, Cengage Learning., 2012.

Barnes, E. A. and Polvani, L.: Response of the midlatitude jets, and of their variability, to increased greenhouse gases in the CMIP5 models, J. Clim., 26(18), 7117–7135, doi:10.1175/JCLI-D-12-00536.1, 2013.

Cohen, J., Screen, J. A., Furtado, J. C., Barlow, M., Whittleston, D., Coumou, D., Francis, J., Dethloff, K., Entekhabi, D., Overland, J. and Jones, J.: Recent Arctic amplification and extreme mid-latitude weather, Nat. Geosci., 7, 627–637,

doi:10.1038/ngeo2234, 2014.

Coumou, D., Petoukhov, V., Rahmstorf, S., Petri, S. and Schellnhuber, H. J.: Quasi-resonant circulation regimes and hemispheric synchronization of extreme weather in boreal summer, Proc. Natl. Acad. Sci., doi:10.1073/pnas.1412797111, 2014.

Dee, D. P., Uppala, S. M., Simmons, A. J., Berrisford, P., Poli, P., Kobayashi, S., Andrae, U., Balmaseda, M. A., Balsamo, G., Bauer, P., Bechtold, P., Beljaars, A. C. M., van de Berg, L., Bidlot, J., Bormann, N., Delsol, C., Dragani, R., Fuentes, M., Geer, A. J., Haimberger, L., Healy, S. B., Hersbach, H., Hólm, E. V., Isaksen, L., Kållberg, P., Köhler, M., Matricardi, M., Mcnally, A. P., Monge-Sanz, B. M., Morcrette, J. J., Park, B. K., Peubey, C., de Rosnay, P., Tavolato, C., Thépaut, J. N. and Vitart, F.: The ERA-Interim reanalysis: Configuration and performance of the data assimilation system, Q. J. R. Meteorol. Soc., 137(656), 553–597, doi:10.1002/qj.828, 2011.

Dijkstra, E. W.: A Note on Two Probles in Connexion with Graphs, Numer. Math., 1(1), 269–271, doi:10.1007/BF01386390, 1959.

Eichelberger, S. J. and Hartmann, D. L.: Zonal jet structure and the leading mode of variability, J. Clim., 20(20), 5149–5163, doi:10.1175/JCLI4279.1, 2007.

Flechsig, M., Böhm, U., Nocke, T. and Rachimow, C.: The Multi-Run Simulation Environment SimEnv, , 1, 2013.

Gallego, D., Ribera, P., Garcia-Herrera, R., Hernandez, E. and Gimeno, L.: A new look for the Southern Hemisphere jet stream, , doi:10.1007/s00382-005-0006-7, n.d.

Grise, K. M. and Polvani, L. M.: The response of midlatitude jets to increased CO2: Distinguishing the roles of sea surface temperature and direct radiative forcing, Geophys. Res. Lett., 41, doi:10.1002/2013GL058489.Received, 2014.

Harnik, N., Galanti, E., Martius, O. and Adam, O.: The anomalous merging of the African and North Atlantic jet streams during the northern hemisphere Winter of 2010, J. Clim., 27(19), 7319–7334, doi:10.1175/JCLI-D-13-00531.1, 2014.

Harnik, N., Garfinkel, C. I. and Lachmy, O.: Dynamics and Predictability of Large-Scale, High-Impact Weather and Climate Events, edited by L. JianPing, S. Richard, G. Richard, and H. Volkert, Cambridge University Press., 2016.

Kirkpatrick, S.: Optimization by simulated annealing: Quantitative studies, J. Stat. Phys., 34, 975–986, doi:10.1007/BF01009452, 1984.

Kretschmer, M., Coumou, D., Donges, J. F. and Runge, J.: Using Causal Effect Networks to analyze different Arctic drivers of mid-latitude winter circulation, J. Clim., 160303130523003, doi:10.1175/JCLI-D-15-0654.1, 2016.

Lee, S. and Kim, H.: The Dynamical Relationship between Subtropical and Eddy-Driven Jets, J. Atmos. Sci., 60(12), 1490–1503, doi:10.1175/1520-0469(2003)060<1490:TDRBSA>2.0.CO;2, 2003.

Li, C. and Wettstein, J. J.: Thermally driven and eddy-driven jet variability in reanalysis, J. Clim., 25(5), 1587–1596, doi:10.1175/JCLI-D-11-00145.1, 2012.

Palmer, T.: Record-breaking winters and global climate change, Science (80-.)., 344(6186), 803–804, doi:10.1126/science.1255147, 2014.

Peings, Y. and Magnusdottir, G.: Forcing of the wintertime atmospheric circulation by the multidecadal fluctuations of the

North Atlantic ocean, Environ. Res. Lett., 9(3), 034018, doi:10.1088/1748-9326/9/3/034018, 2014.

Pena-Ortiz, C., Gallego, D., Ribera, P., Ordonez, P. and Del Carmen Alvarez-Castro, M.: Observed trends in the global jet stream characteristics during the second half of the 20th century, J. Geophys. Res. Atmos., 118, 2702–2713, doi:10.1002/jgrd.50305, 2013.

Petoukhov, V., Rahmstorf, S., Petri, S. and Schellnhuber, H. J.: Quasiresonant amplification of planetary waves and recent Northern Hemisphere weather extremes., Proc. Natl. Acad. Sci. U. S. A., 110(14), 5336–41, doi:10.1073/pnas.1222000110, 2013.

Petoukhov, V., Petri, S., Rahmstorf, S., Coumou, D., Kornhuber, K. and Schellnhuber, H. J.: The role of quasi-resonant planetary wave dynamics in recent boreal spring-to-autumn extreme events, Prep., 113(25), 6862–6867, doi:10.1073/pnas.1606300113, 2016.

Rikus, L.: A simple climatology of westerly jet streams in global reanalysis datasets part 1 : mid ‐ latitude upper tropospheric jets, Clim. Dyn., doi:10.1007/s00382-015-2560-y, 2015.

Solomon, A. and Polvani, L. M.: Highly Significant Responses to Anthropogenic Forcings of the Midlatitude Jet in the Southern Hemisphere, J. Clim., 29(9), 3463–3470, doi:10.1175/JCLI-D-16-0034.1, 2016.

Son, S.-W. and Lee, S.: The Response of Westerly Jets to Thermal Driving in a Primitive Equation Model, J. Atmos. Sci., 62(10), 3741–3757, doi:10.1175/JAS3571.1, 2005.

Stadtherr, L., Coumou, D., Petoukhov, V., Petri, S. and Rahmstorf, S.: Record Balkan floods of 2014 linked to planetary wave resonance, Sci. Adv., (April), (minor revisions), doi:10.1126/sciadv.1501428, 2016.

Trenberth, K. E., Fasullo, J. T., Branstator, G. and Phillips, A. S.: Seasonal aspects of the recent pause in surface warming, Nat. Clim. Chang., 4(October), 911–916, doi:10.1038/nclimate2341, 2014.

Woollings, T.: Dynamical influences on European climate: an uncertain future., Philos. Trans. A. Math. Phys. Eng. Sci., 368(1924), 3733–3756, doi:10.1098/rsta.2010.0040, 2010.

Woollings, T., Hannachi, A. and Hoskins, B.: Variability of the North Atlantic eddy-driven jet stream, , (April), 856–868, doi:10.1002/qj.625, 2010.

Figures

Earth Syst. Dynam. Discuss., doi:10.5194/esd-2016-37, 2016
Manuscript under review for journal Earth Syst. Dynam.
Published: 29 August 2016

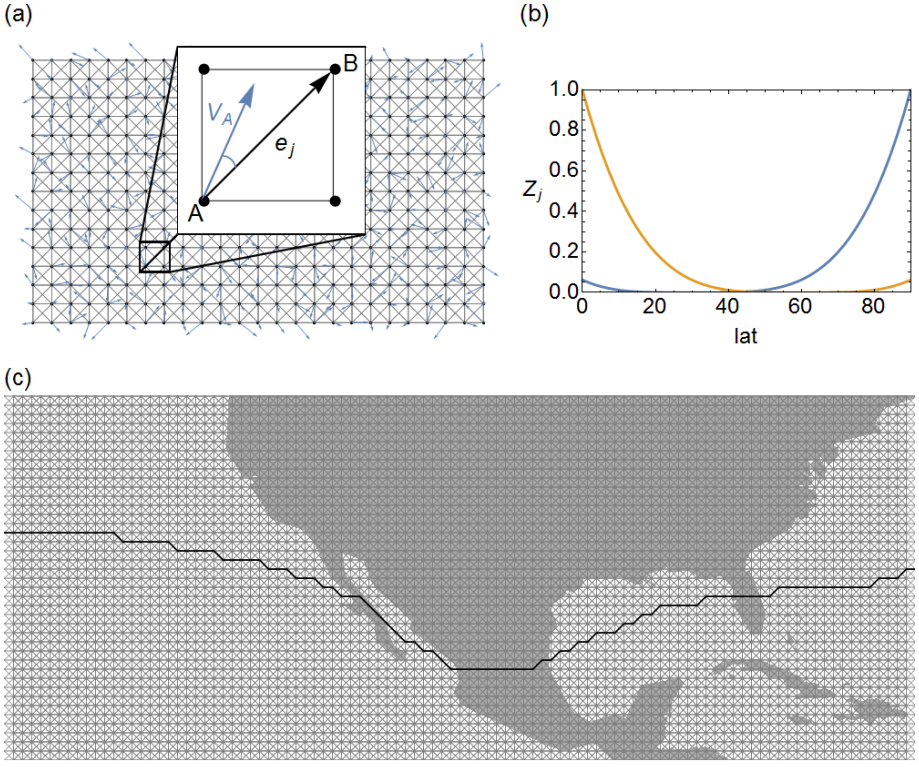

Figure 1. Definition of edge costs: (a) shows all nodes and edges as well as the wind velocities of the considered node (blue arrows) in the grid. The edge costs are computed from wind velocities (length of blue arrows, X_j), wind direction (angle between blue arrow and black edge, Y_j) as well as the latitudinal position Z_j. (b) indicates the third cost term Z_j of the STJ (blue) and PFJ (orange). The edge cost is very low in the vicinity of $\phi_{clim} = 30°N$ for the STJ and $\phi_{clim} = 60°N$ for the PFJ and very high far away of ϕ_{clim}. (c) shows the STJ (black line) in the network graph over North- and Central America for a certain time step.

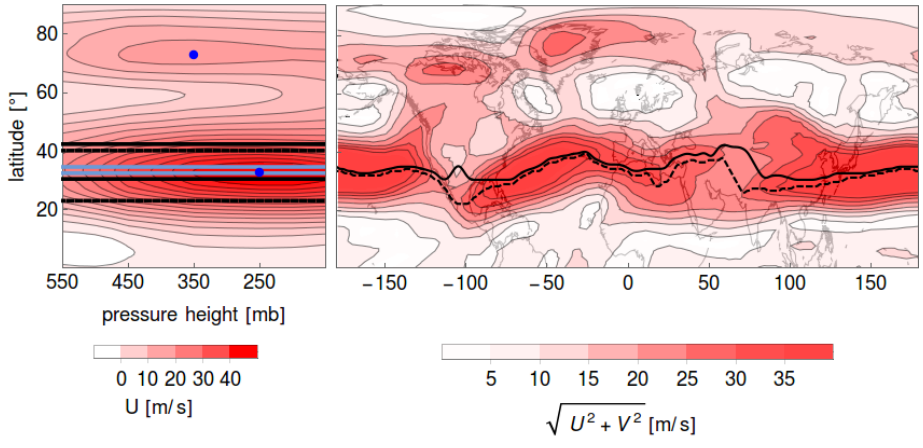

Earth Syst. Dynam. Discuss., doi:10.5194/esd-2016-37, 2016
Manuscript under review for journal Earth Syst. Dynam.
Published: 29 August 2016

Earth System Dynamics Discussions
Open Access
EGU

Figure 2. Left panel: Zonal mean latitude of the jet stream core calculated with Dijkstra's algorithm using untuned weights (light blue lines) and that computed with Rikus' algorithm (blue circles). The black solid (dashed) lines are the borders of the PFJ (STJ) core latitude positions as calculated with Dijkstra's algorithm. Right panel: polar (black) and subtropical (black dashed) jet stream cores are shown. (15 days running mean around 13.01.2010).

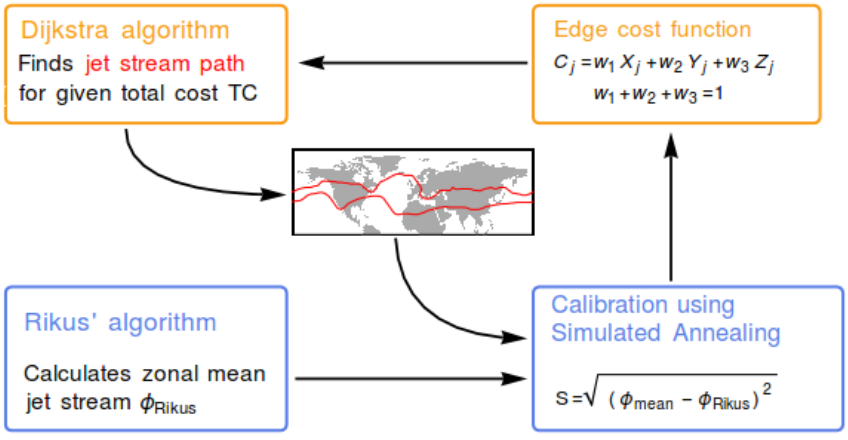

Figure 3. Calibration Scheme. Before calculating the shortest path with Dijkstra's algorithm, the cost of each edge has to be calculated according to the three terms X_j, Y_j and Z_j. In order to find the correct weights of the terms, we calibrate them with Simulated Annealing and using Rikus' algorithm to construct the skill function.

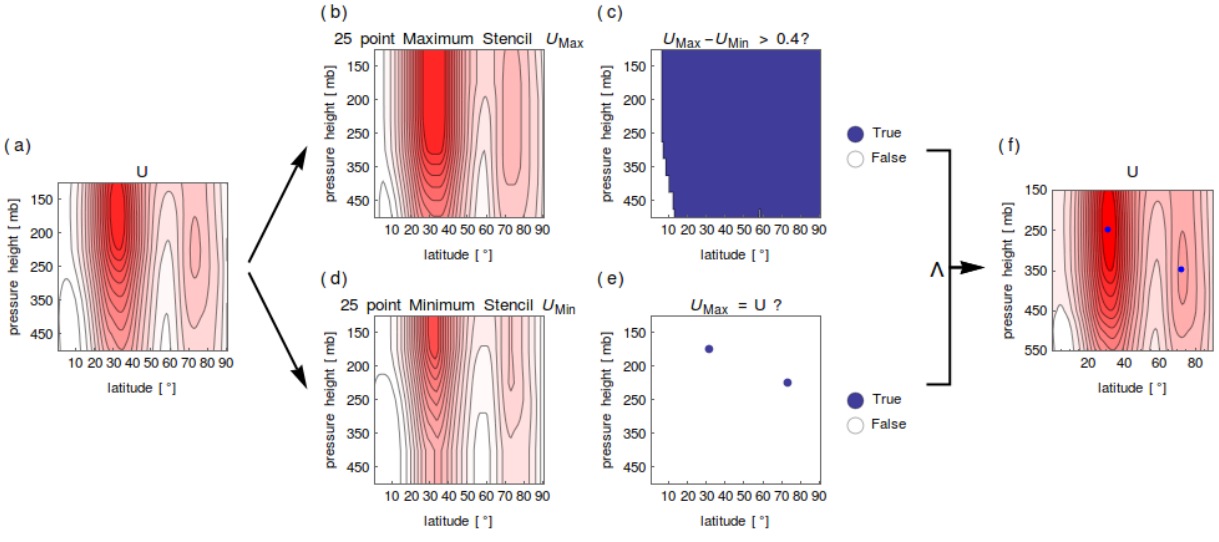

Figure 4. Rikus' Scheme. In (b) the 25 point maximum stencil (U_{Max}) and in (d) the 25 point minimum (U_{Min}) stencil from (a) is calculated. In (d) the condition $U_{Max}(x,y) - U_{Min}(x,y) > 0.4$ and in (e) the condition $U_{Max}(x,y) = U(x,y)$ is examined. Only those points, where both conditions are fulfilled, are zonal mean jet stream cores (f, white points).

Earth Syst. Dynam. Discuss., doi:10.5194/esd-2016-37, 2016
Manuscript under review for journal Earth Syst. Dynam.
Published: 29 August 2016

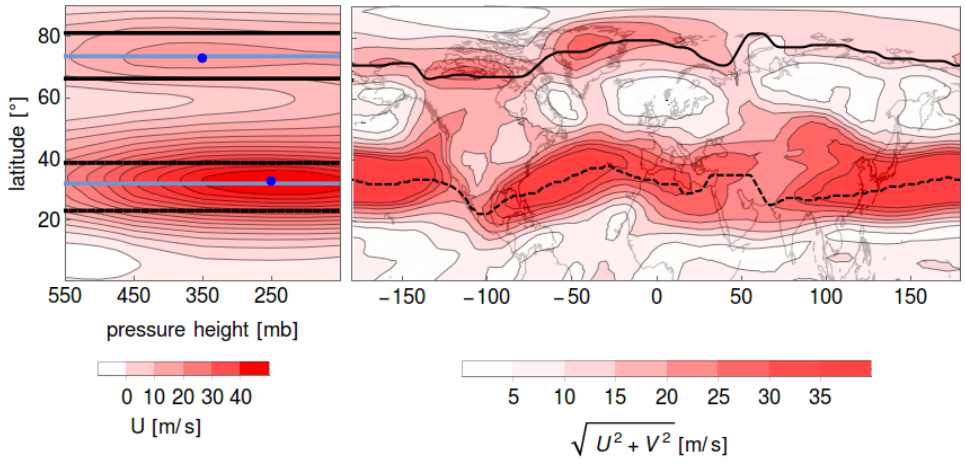

Figure 5 15 days running mean around 13.01.2010, jet stream cores calculated with Dijkstra's algorithm using optimized weights (compare Fig. 6).

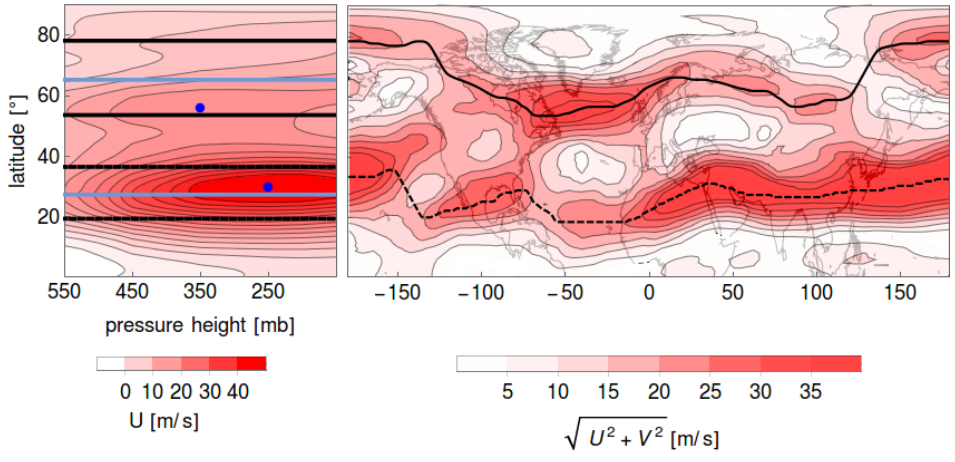

Figure 6. 15 days running mean around 02.03.1979 , compare Fig. 2. The right panel shows three maxima (30°N, 50°N and 75°N), because of that the mean jet stream core found with Dijkstra's algorithm (light blue line) does not match with the jet stream core found by Rikus' algorithm (blue circle).

Earth Syst. Dynam. Discuss., doi:10.5194/esd-2016-37, 2016
Manuscript under review for journal Earth Syst. Dynam.
Published: 29 August 2016

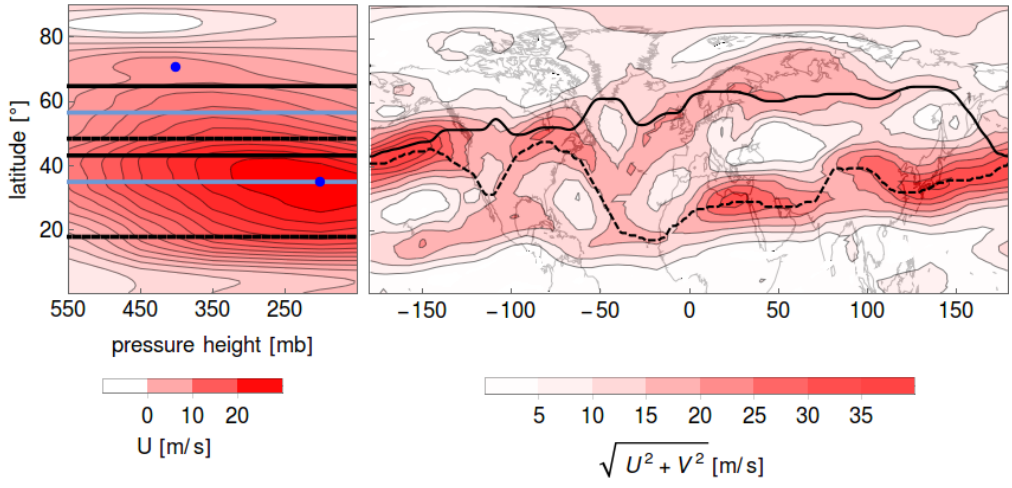

Figure 7. There is only a maximum in the wind field in the region between $0°E - 100°E$ and around $70°N$ latitude and for that reason the PFJ core found with Dijkstra's algorithm (light blue line) does not match with the PFJ core found by Rikus' algorithm (blue circle.) (15 days running mean around 12.05.1979, compare Fig. 2).

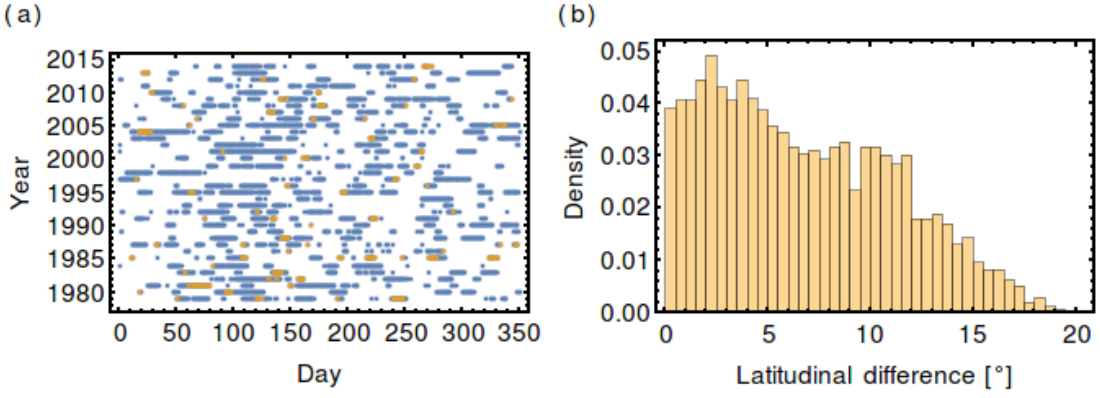

Figure 8. (a) Day-year plot showing days used for tuning (blue) and those days, where Rikus' latitude position is not within the range of latitudes found with Dijkstra's algorithm (199 of 3122 datapoints, 6.4%), (b) Histogram of minimum latitudinal difference between the jet stream core found with Dijkstra's algorithm and the mean latitude from Rikus' algorithm, in degrees, for the polar jet stream.

Earth Syst. Dynam. Discuss., doi:10.5194/esd-2016-37, 2016
Manuscript under review for journal Earth Syst. Dynam.
Published: 29 August 2016

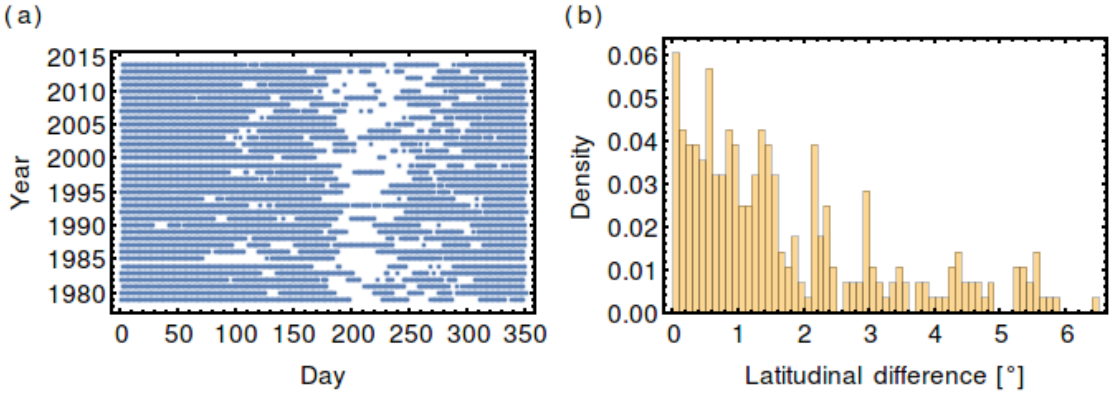

Figure 9. (a) Day-year plot for the subtropical jet stream detection scheme (compare Fig. 8) , (b) Histogram of minimum latitudinal difference between the jet stream core found with Dijkstra's algorithm and the mean latitude from Rikus' algorithm, in degrees, for the polar jet stream

Earth Syst. Dynam. Discuss., doi:10.5194/esd-2016-37, 2016
Manuscript under review for journal Earth Syst. Dynam.
Published: 29 August 2016

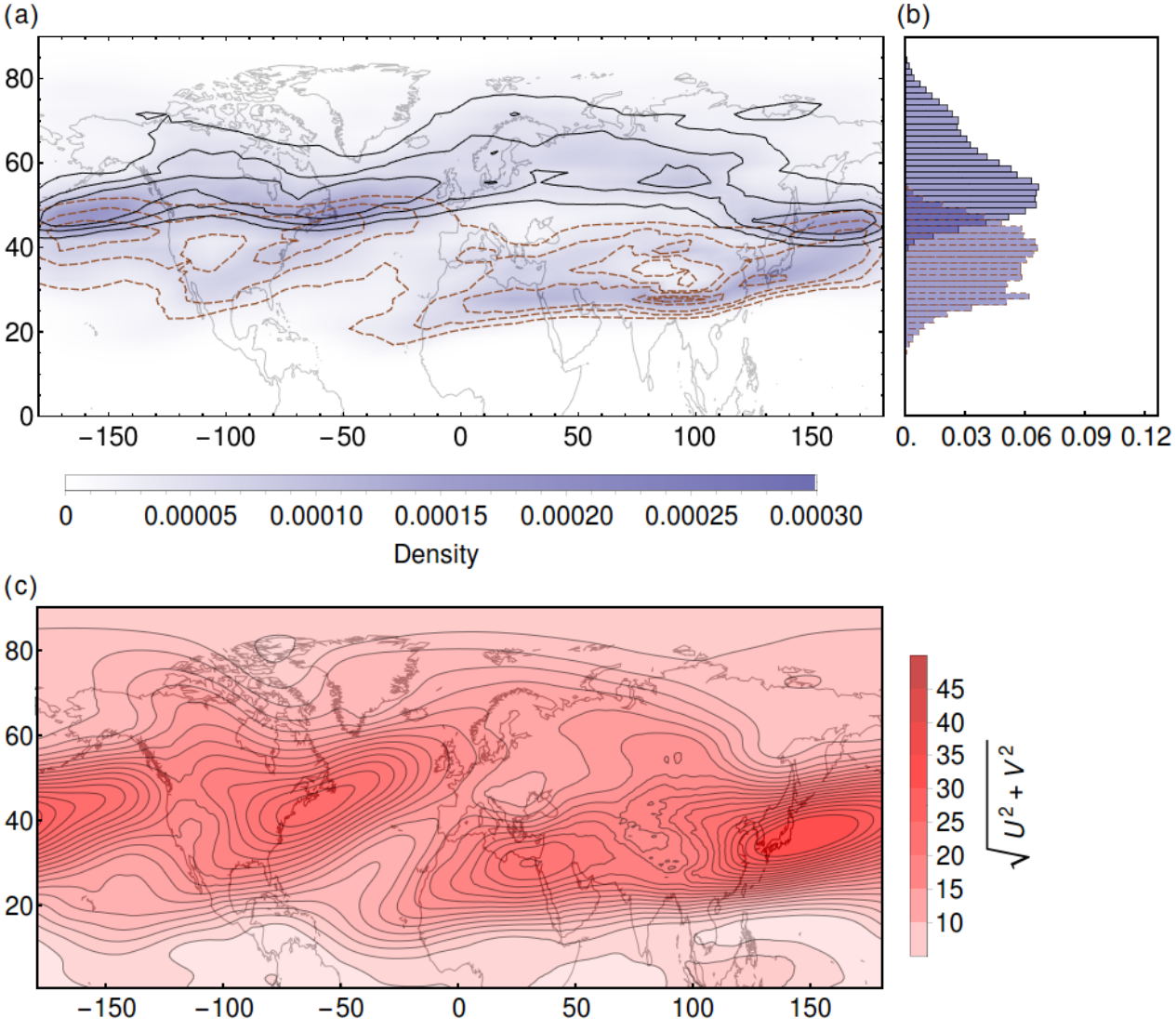

Figure 10. Probability analysis: (a) and (b) show the annual probability density plot and a histogram of the jet stream occurrences (1979-2014). The brown dashed contour lines represent the subtropical jet stream, whereas the black solid contour lines represent the polar jet stream. (c) depicts the climatological annual wind field (averaged over 1979-2014).

Earth Syst. Dynam. Discuss., doi:10.5194/esd-2016-37, 2016
Manuscript under review for journal Earth Syst. Dynam.
Published: 29 August 2016

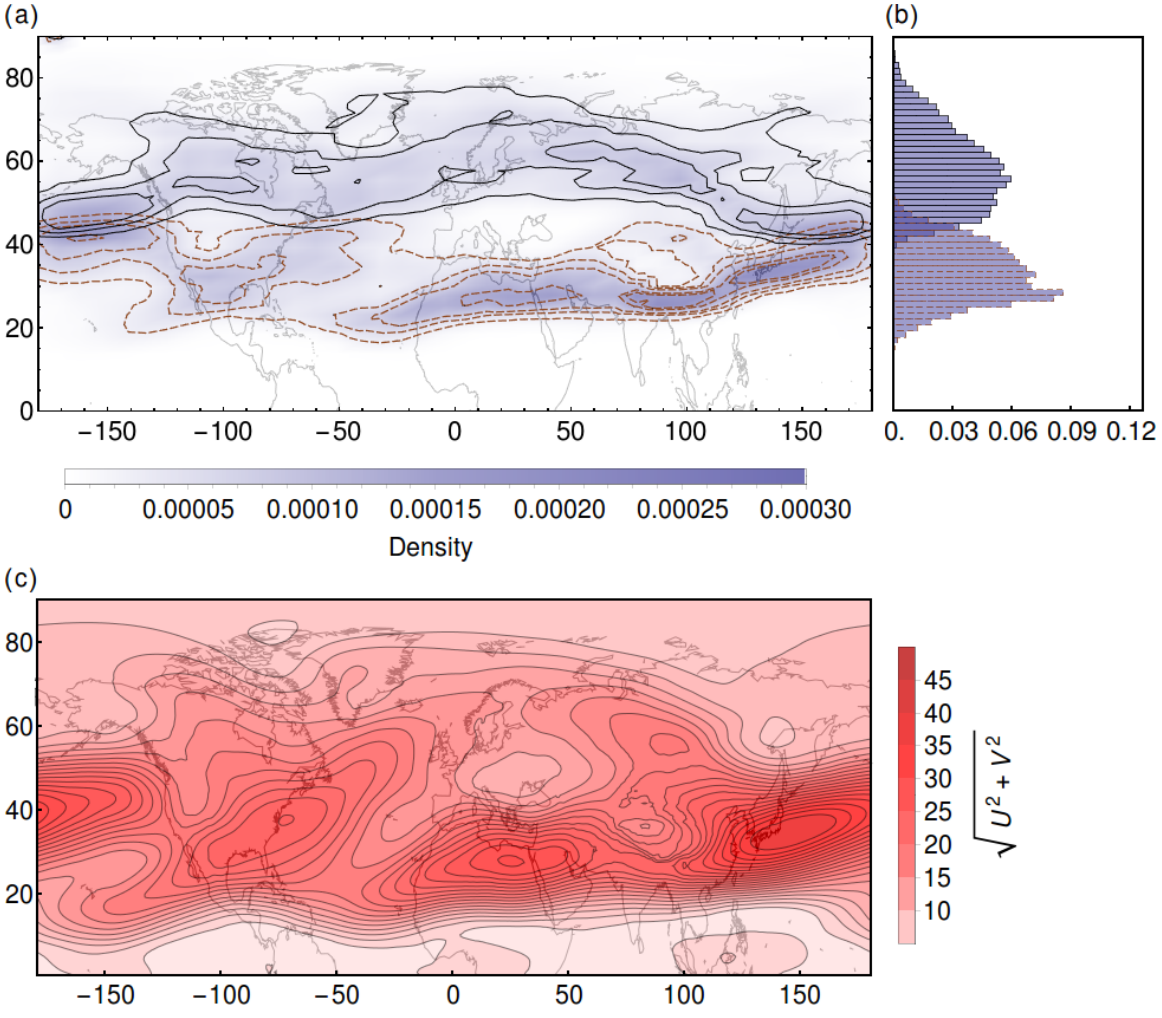

Figure 11. Probability analysis for spring months (MAM, compare Fig 10).

Earth Syst. Dynam. Discuss., doi:10.5194/esd-2016-37, 2016
Manuscript under review for journal Earth Syst. Dynam.
Published: 29 August 2016

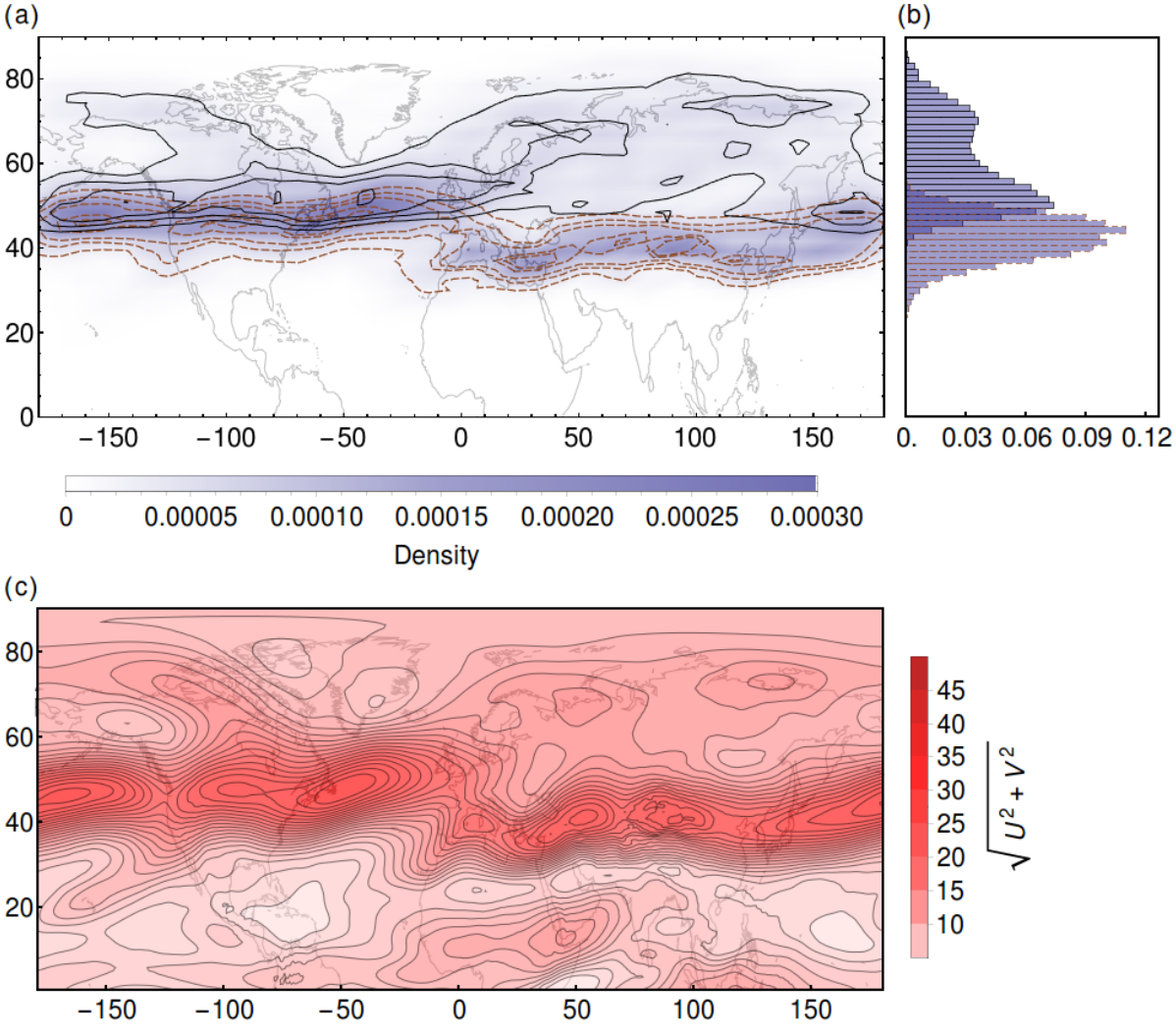

Figure 12. Probability analysis for summer months (JJA, compare Fig 10).

Earth Syst. Dynam. Discuss., doi:10.5194/esd-2016-37, 2016
Manuscript under review for journal Earth Syst. Dynam.
Published: 29 August 2016

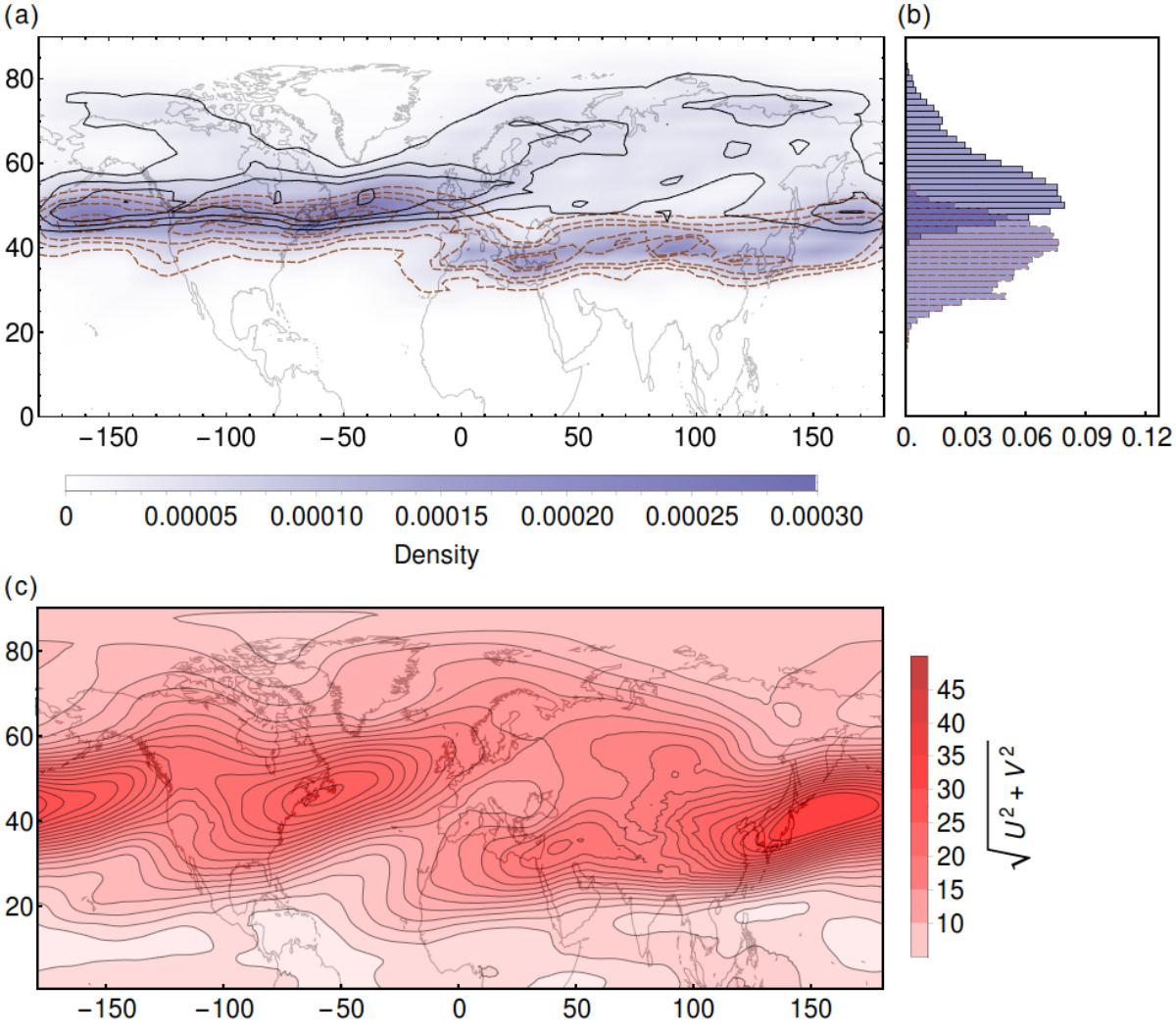

Figure 13. Probability analysis for autumn months (SON, compare Fig 10).

Earth Syst. Dynam. Discuss., doi:10.5194/esd-2016-37, 2016
Manuscript under review for journal Earth Syst. Dynam.
Published: 29 August 2016

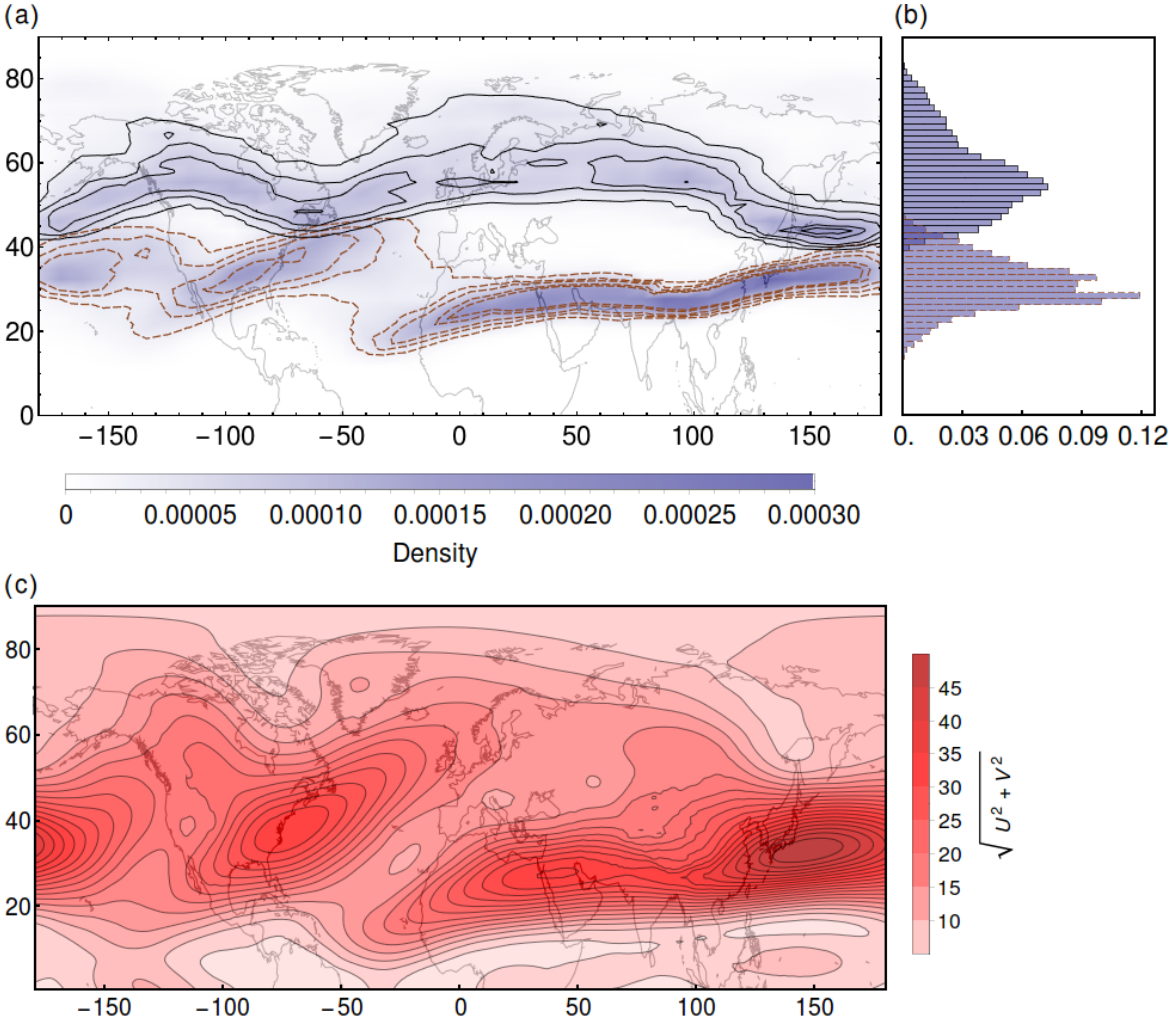

Figure 14. Probability Analysis for winter months (DJF, compare Fig 10).

Tables

Table 1 Start and optimized jet stream parameters used for the edge cost function

Season	Parameters	Subtropical jet stream		Polar jet stream	
		Start	Optimized	Start	Optimized
cold	w_1	0.49	0.044	0.49	0.044
	w_2	0.0015	-	0.0015	-
	w_3	0.5	0.95	0.5	0.95

Earth Syst. Dynam. Discuss., doi:10.5194/esd-2016-37, 2016
Manuscript under review for journal Earth Syst. Dynam.
Published: 29 August 2016

	ϕ_{clim}	30°N	25.1°N	60°N	67.5°N
warm	w_1	0.49	0.072	0.49	0.043
	w_2	0.0015	-	0.0015	-
	w_3	0.5	0.92	0.5	0.95
	ϕ_{clim}	30°N	29.8°N	60°N	69.1°N